temperature of about 1900 K (*25*). The *H*-band magnitude of Kelu 1 at a distance of 12 pc would correspond to a mass of approximately of 0.065 $M_\odot$ for an age of 0.5 Gy (0.07 $M_\odot$ for an age of 1 Gy). In Fig. 2, we have converted magnitude differences to masses, using current evolutionary models for brown dwarfs and giant planets (*26*). A planet with a mass of about 7 M_J orbiting Kelu 1 at a separation larger than 4 AU would have been detected. For an age of 1 Gy, the detection limit would rise to a companion with 20 M_J at 4 AU. The age dependence of mass limits as a function of magnitude difference limits is illustrated by the comparison between the solid line (0.5 Gy) and the dashed line (1.0 Gy) in Fig. 2. The example of Kelu 1 shows that it is feasible to detect superplanets with masses in the range of 5 to 10 M_J with direct imaging in orbit around nearby young BD primaries if they have separations that are typical of the giant planets in the solar system (5 to 30 AU).

References and Notes

1. See S. R. Kulkarni, *Science* **276**, 1350 (1997) for a recent review.
2. 0.075 $M_\odot$ is the minimum mass that allows stable hydrogen burning to develop in a stellar core within one Hubble time [I. Baraffe, G. Chabrier, F. Allard, P. H. Hauschildt, *Astron. Astrophys.* **337**, 403 (1998)].
3. 0.013 $M_\odot$ is the minimum mass for deuterium burning (the most fragile element) for solar metallicity [A. Burrows, D. Saumon, T. Guillot, W. B. Hubbard, J. I. Lunine, *Nature* **375**, 299 (1995)].
4. G. Basri and G. W. Marcy, in *Star Formation Near and Far*, S. S. Holt and L. G. Mundy, Eds. (AIP Press, New York, 1997), pp. 228–240; B. Oppenheimer, S. R. Kulkarni, J. R. Stauffer, in *Protostars and Planets IV*, V. Mannings, A. Boss, S. Russell, Eds. (Univ. of Arizona Press, Tucson, AZ, in press).
5. R. Rebolo, M. R. Zapatero Osorio, E. L. Martín, *Nature* **377**, 129 (1995).
6. T. Nakajima *et al.*, *ibid.* **378**, 463 (1995).
7. The "lithium test" was proposed by R. Rebolo, E. L. Martín, and A. Magazzù [*Astrophys. J.* **389**, L83 (1992)] as a method to distinguish between stars and BDs; it was further developed and applied to BD candidates for the first time by A. Magazzù, E. L. Martín, and R. Rebolo [*ibid.* **404**, L17 (1993)] and finally met with success in the Pleiades BD candidates PPl 15 [G. Basri, G. W. Marcy, J. R. Graham, *ibid.* **458**, 600 (1996)] and Teide 1 [R. Rebolo, E. L. Martín, G. Basri, G. W. Marcy, M. R. Zapatero Osorio, *ibid.* **469**, L53 (1996)]. All the free-floating BDs known so far in clusters and in the field have been confirmed by the presence of lithium.
8. The only known BD whose substellar status does not need a lithium confirmation is Gl 229B, because the presence of CH_4 indicates that it is too cool to be a star [B. R. Oppenheimer, S. R. Kulkarni, K. Matthews, T. Nakajima, *Science* **270**, 1478 (1995)].
9. M. T. Ruiz, S. K. Leggett, F. Allard, *Astrophys. J.* **491**, L107 (1997).
10. F. Garzón, E. Epchtein, A. Omont, B. Burton, P. Persi, Eds., *The Impact of Large Scale Near-IR Sky Surveys* (vol. 210 of the Astrophysics and Space Science Library Series, Kluwer Academic, Dordrecht, Netherlands, 1997).
11. X. Delfosse *et al.*, *Astron. Astrophys.* **327**, L25 (1997).
12. E. E. Becklin and B. Zuckerman, *Nature* **336**, 658 (1988).
13. E. L. Martín, G. Basri, X. Delfosse, T. Forveille, *Astron. Astrophys.* **327**, L29 (1997); C. G. Tinney, X. Delfosse, T. Forveille, *ibid.* **338**, 1066 (1998).
14. R. I. Thompson, M. J. Rieke, G. Schneider, D. Hines, M. R. Corbin, *Astrophys. J.* **492**, L95 (1998).
15. *HST Data Handbook*, Version 3.0, Vol. I, M. Voit, Ed. (Space Telescope Science Institute, Baltimore, MD, 1997).
16. H. C. Harris, C. C. Dahn, D. G. Monet, in *Proceedings of ESA Symposium "Hipparcos-Venice 97"* [ESA-SP **402**, 105 (1997)].
17. R. Rebolo *et al.*, *Science* **282**, 1309 (1998).
18. D. A. Golimowski, C. J. Burrows, S. R. Kulkarni, B. R. Oppenheimer, R. A. Bruckardt, *Astron. J.* **115**, 2579 (1998).
19. G. W. Marcy, W. D. Cochran, M. Mayor, in *Protostars and Planets IV*, V. Mannings, A. Boss, S. Russell, Eds. (Univ. of Arizona Press, Tucson, AZ in press).
20. K. L. Luhman, J. Liebert, G. H. Rieke, *Astrophys. J.* **489**, L165 (1997); C. Briceño, L. Hartmann, J. R. Stauffer, E. L. Martín, *Astron. J.* **115**, 2074 (1998); M. Tamura, Y. Itoh, Y. Oasa, T. Nakajima, *Science* **282**, 1095 (1998).
21. M. W. Pound and L. Blitz, *Astrophys. J.* **444**, 270 (1995). F. Motte, P. André, R. Neri, *Astron. Astrophys.* **336**, 150 (1998).
22. B. A. Wilking, T. P. Greene, M. Meyer, *Astrophys. J.*, in press.
23. O. Malkov, A. Piskunov, H. Zinnecker, *Astron. Astrophys.* **338**, 452 (1998).
24. E. L. Martín *et al.*, *Astrophys. J.* **509**, L113 (1998).
25. G. Basri *et al.*, in *The Tenth Cambridge Workshop on Cool Stars, Stellar Systems and the Sun*, R. A. Donahue and J. A. Bookbinder, Eds. (Astronomical Society of the Pacific Conference Series 154, 1998), pp. 1819–1827.
26. We used the *H*-band brightness provided by A. Burrows *et al.* [*Astrophys. J.* **491**, 856 (1997)] for masses between 1 and 40 M_J and ages of 0.5 and 1.0 Gy.

27. This paper is based on observations made with the NASA/ESA Hubble Space Telescope, obtained at the Space Telescope Science Institute, which is operated by the Association of Universities for Research in Astronomy under NASA contract NAS5-26555. We thank the director of the Space Telescope Science Institute for granting us HST Director Discretionary time. G.B. acknowledges the support of NSF through grant AST96-18439. E.L.M. was supported by a postdoctoral fellowship of the Spanish Ministerio de Educación y Cultura.

17 December 1998; accepted 2 February 1999

"Debye-Scherrer Ellipses" from 3D Fullerene Polymers: An Anisotropic Pressure Memory Signature

L. Marques,[1] M. Mezouar,[2] J.-L. Hodeau,[3]* M. Núñez-Regueiro,[4] N. R. Serebryanaya,[5] V. A. Ivdenko,[5] V. D. Blank,[6] G. A. Dubitsky[6]

High-pressure studies on fullerenes have previously shown the existence of one- and two-dimensional (2D) polymerized C_{60} structures. Synchrotron radiation measurements, performed on C_{60} samples quenched from 13 gigapascals and 820 kelvin, yield unambiguous proof for the existence of a three-dimensional (3D) polymerized C_{60} derivative. Moreover, unusual ellipsoidal Debye-Scherrer diffraction patterns are observed, which shows that the giant anisotropic deformation induced by the nonhydrostatic compression is retained in the quenched samples. The multiple bonding possibilities of the highly symmetrical C_{60} allow the retention (down to ambient pressure) of the deformation, a phenomenon reported previously only under high pressure.

Under high pressures, unsaturated organic molecules are particularly prone to cross-linking reactions resulting in denser, more saturated species (*1*). Fullerene molecules are no exception, and C_{60} molecules have been shown to polymerize at high pressure and temperature (*2, 3*). Bonding through 2+2 cycloaddition reactions of each molecule with its two neighbors in the <110> direction of the face-centered cubic (fcc) structure leads to the formation of a one-dimensional (1D) material with linear chains of polymerized C_{60} molecules (*2*). Further bonding of these chains to their next nearest neighbors in the (001) plane results in a 2D tetragonal (2D-T) polymerized phase in which each molecule is bonded to four neighbors; if the bonding between chains proceeds within the high-density (111) plane, the resulting 2D polymerized phase is rhombohedral (2D-R) and each molecule is bonded to six neighbors. In spite of the conceptual prediction (*4, 5*) and favorable stability analysis of several 3D structures (*5*), 1D and 2D phases have, to date, remained the only polymerized phases to be detected and identified for pressures below 8 GPa at all temperatures (*6*). Experiments at higher pres-

[1]Departamento de Física, Universidade de Aveiro, 3800 Aveiro, Portugal. [2]European Synchrotron Radiation Facility, 38041 Grenoble, France. [3]Laboratoire de Cristallographie, CNRS, Boite Postale 166 Cedex 09, 38042 Grenoble, France. [4]Centre de Recherches sur les Très Basses Températures, CNRS, Boite Postale 166 Cedex 09, 38042 Grenoble, France. [5]Institute of Spectroscopy RAS, Troitsk Moscow Region, 142092 Russia. [6]Research Center for Superhard Materials, 7-a Centralnaya Street, Troitsk Moscow Region, 142092 Russia.

*To whom correspondence should be addressed. E-mail: hodeau@polycnrs-gre.fr

sures have yielded cage-breaking transformations to graphitic material (*7*), diamond (*8, 9*), amorphous sp^3 carbon (*10, 11*), or ultrahard phases (*12*), and evidence of distortions from fcc in these latter phases was reported from analysis of transmission electron microscopy images (*13*). We describe detailed x-ray synchrotron measurements on samples obtained in a similar way as those of (*12*), providing evidence for a 3D polymerized C_{60} derivative that can be quenched to ambient conditions.

We compressed C_{60} powder to 13 GPa in a toroid-type chamber, then heated it at 820 K for 1 min; the pressure was released when the sample had cooled to room temperature (*12*). The 2D diffraction patterns of the quenched samples were taken in transmission geometry on the ID30 beamline at the European Synchrotron Radiation Facility (ESRF) (*14*). We used short wavelengths (λ = 0.3738 and 0.5120 Å) and a small beam size (0.3 mm by 0.6 mm) in two different experiments and settings. Complete powder spectra were collected using a fast-scan image plate detector (*15*) placed at different distances (134 to 400 mm) from the sample. The image plate (IP) perpendicularity to the incident x-ray beam was checked using the diffraction pattern from a silicon powder as reference. The IP tilts were very weak (less than 0.35°) and were corrected using the Fit2D program (*16*). The spatial distortion due to the nonlinearity of the IP response was taken into account in all analyzed images. This procedure, currently in use at the ESRF on different beamlines, ensures that the measured effects can be attributed exclusively to the C_{60} samples.

Diffraction images were taken at different beam directions relative to the loading direction of compression during synthesis (Fig. 1). The continuous loci of the Bragg reflections of Fig. 1A are elliptical and not circular as expected for normal powder Debye-Scherrer (D-S) patterns obtained with a 2D detector placed perpendicular to the beam axis. For the same bulk sample, the elliptical shape of D-S patterns varies depending on its orientation and can reach nearly perfect circles (Fig. 1C). The images obtained for different sample orientations correspond to an oblate ellipsoid in reciprocal space. The patterns shown (Fig. 1) correspond to the two sections (orientations) that characterize the strain ellipsoid. The 1D diffraction profiles extracted along any arbitrary radial (or azimuthal) direction from these spectra can be indexed as a compressed fcc fullerite lattice. The cell parameter of these D-S ellipses varies continuously with the radial direction (Ψ), ranging from 11.3 to 12.6 Å. These values were confirmed by conventional measurements taken with a Cu Kα x-ray tube in a reflection geometry. Similar diffracted ellipses, albeit with a much smaller deformation, have previously been observed only in pressure experiments with in situ x-ray spectra acquisition (*17, 18*). These ellipsoidal patterns are a result of the anisotropic stress (that is, a deviatoric stress) caused by the uniaxial force that is used to establish the pressure. The elliptical shape results from a larger compression of the crystallographic lattice parameters in the direction of the applied force, because the magnitude of each interplanar spacing d_{hkl} is a function of its orientation with respect to the stress field within the sample (*19*). The polymerized fullerene samples were produced under nonhydrostatic conditions, and therefore, we must conclude that the stress gradient under which they were made remains recorded in the quenched samples. The orientation of the uniaxial stress is unique in the bulk sample, and depending upon its orientation relative to that of the x-ray beam, different anisotropic patterns are observed. The intensities of our ellipses are quasi-continuous, implying that the bulk sample is polycrystalline with some texture, the deformation in each grain having a different orientation with respect to its crystal lattice.

In usual molecular materials, the constituent molecules have few available bonding directions, and only the grains in which these particular directions are favorably aligned with respect to the stress will have the possibility of maintaining the metastable high-pressure structure upon quenching. It is the high symmetry of the C_{60} molecule, with 30 isotropically distributed equivalent bonding directions, that allows the retention of the nonuniform deformation in the quenched sample. Along the direction where the highest stress is present during the phase transformation, the molecules are drawn closer, allowing more or stronger intermolecular covalent bonds to be formed. Consequently, the d_{hkl} spacing remains the smallest in this particular direction. Once the pressure is released, these new intermolecular covalent bonds preserve the deformation induced by the anisotropic stress application to the sample.

The retention of the large high-pressure deformation in the quenched sample suggests a structure with C_{60} molecules bonded in 3D space (to several of the 12 nearest neighbors in the fcc lattice). Some of the simplest 3D polymerized fullerite phases proposed in the literature are shown in Fig. 2). The first type, 3D-R, is formed by bonding of 2D-R layers (Fig. 2, A and B) (*5*). The second type, 3D-T, is obtained

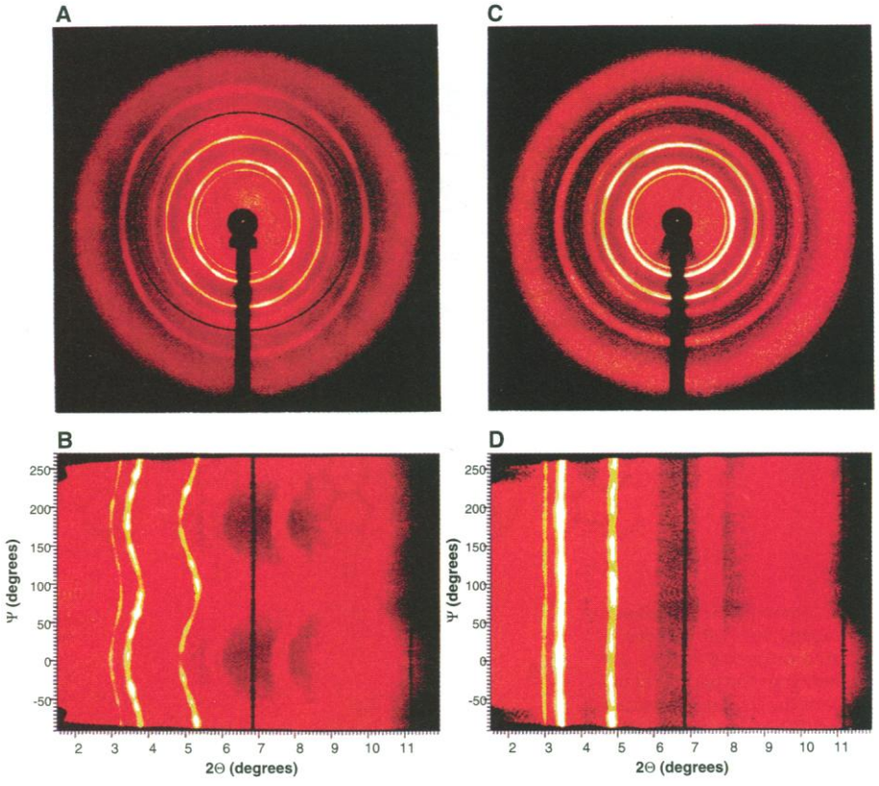

Fig. 1. Diffraction images showing (**A** and **B**) the elongated elliptical shape of the D-S rings obtained when the beam direction is nearly perpendicular to the uniaxial direction of compression during synthesis, and (**C** and **D**) the circular shape of the D-S rings obtained when the beam direction nearly coincides with this uniaxial direction of compression. (A) cuts the ellipsoid at its meridian, and (C) is the circular section of the ellipsoid at its equator. (B) and (D) are an unrolled projection of the corresponding D-S ring [(A) and (C), respectively] along an azimuthal line (an entire ring corresponds to a 360° variation of the azimuthal angle Ψ). The eccentricity of the diffracted ellipse can be estimated by its difference relative to perfect lines at a given 2Θ angle. The sample spectra are shown with the corresponding silicon reference spectrum to emphasize their ellipse eccentricity. The huge circular diffuse scattering is due to the coexistence of the carbon amorphous phase, which becomes dominant at synthesis temperature above 1100 K; this amorphous phase has not retained the anisotropic deformation.

by bonding of 2D-T planes (Fig. 2, C and D) and is derived, with less compression along the c axis, from the structure proposed by O'Keeffe (*4*). In both cases, the intralayer bonding continues to be of the 2+2 type, but the detailed stacking and interlayer bonding differs, resulting in distinct but almost equivalent structures (*5*) where the maximum compression must be normal to the layers. The last structure, 3D-C (3D cubic), of this nonexhaustive list (Fig. 2, E and F) is the result of 2+4 bonding (*20*) of each molecule with its 12 nearest neighbors in the simple cubic high-pressure phase, where the double bonds of one molecule face a hexagon (*21*) of its neighbor [that is, the "H" phase in (*22*)].

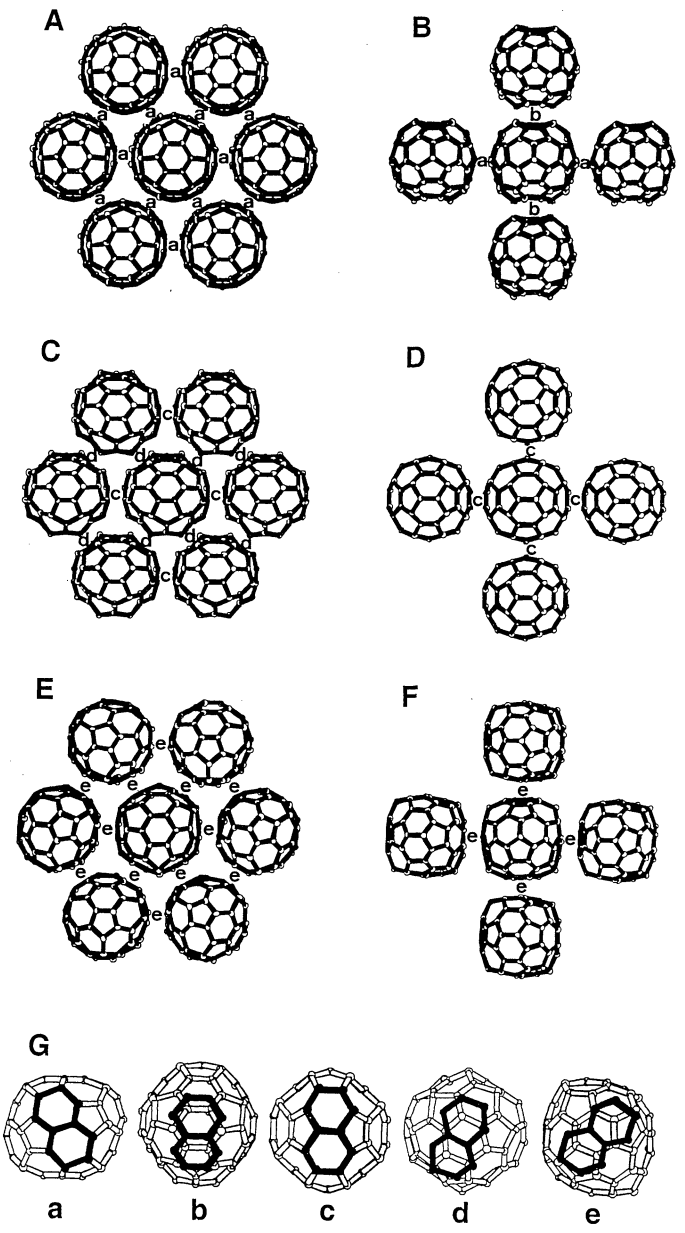

Fig. 2. Projections on (111) and (001) fcc planes of the distorted C_{60} molecules for three 3D polymerized models (**A** and **B**) 3D-R derived from the 2D-R structure (*2*), (**C** and **D**) 3D-T derived from the 2D-T structure (*2*), and (**E** and **F**) 3D-C derived from the high-pressure phase with hexagon–double bond orientational ordering (*22*). These representations use cell parameters and molecular deformations compatible with the anisotropy and intensities of the D-S ellipses. The different types of intermolecular bonding (a, b, c, d, e) shown in (**G**) illustrate the relative position of atoms in neighboring molecules, where the bold carbon cycles represent the two carbon hexagons which face the adjacent molecule.

Let us now analyze the nature of the compressed fullerite state. If we apply an inverse geometrical transformation along the uniaxial axis to the crystalline lattice, it can be treated as a cubic fcc structure. For each grain, Bragg peaks are on D-S ellipsoids (Fig. 3A) and correspond to a specific distortion of the cubic lattice. This distortion is huge ($\Delta a/a \sim 9\%$), and the shortest lattice parameter is along the direction of the uniaxial pressure applied during the phase transformation of the powder sample. From grain to grain, this direction varies relative to its crystallographic orientation. In the particular case where this direction coincides with a high-symmetry axis, the grain develops some of the structures described above. For example, if the grain is oriented with its <111> (or <001>) direction along the uniaxial pressure axis, its deformation is rhombohedral 3D-R (Fig. 3B) [or tetragonal 3D-T (Fig. 3C)]. The hkl Bragg reflections contribute punctually to the D-S ellipses (Fig. 3A); moreover, to obtain continous ellipses from the Bragg reflections originating from different grains, the deformation in each grain must yield the same volume per molecule.

The lattice parameters of the 3D distorted C_{60} phases are obtained from the size and eccentricity of the ellipses (Table 1). It must be noted that they could vary slightly with the area analyzed by the x-ray beam, indicating some radial deformation gradient in the bulk sample. The measured lattice parameters yield a very small volume per molecule (437 to 464 Å^3) and a giant anisotropy of the cell (8 to 10%). This volume is lower than in pristine C_{60} (709 Å^3) and in 1D and 2D fullerite polymers (650 Å^3

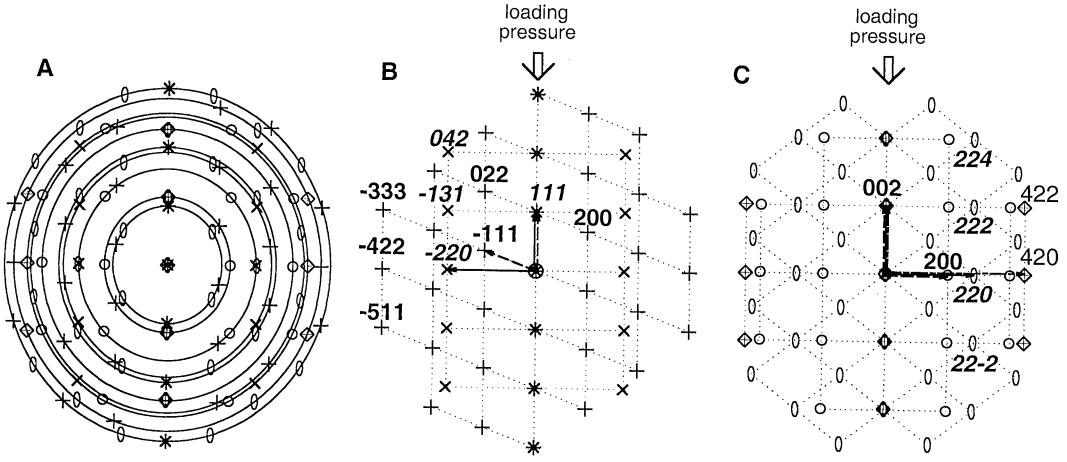

Fig. 3. Schemes of D-S ellipses (**A**) superposed with nodes of distorted reciprocal lattices corresponding to the particular cases where the loading pressure is applied (**B**) along the <111> direction (rhombohedral distortion) or (**C**) along the <001> direction (tetrahedral distortion). Bold, italic, or standard indices and various crosses or nodes correspond to different reciprocal planes. Cell parameters correspond to those given in Table 1.

and 618 to 597 Å^3, respectively) (*2*), and is compatible with a structure containing intact (though probably deformed) fullerene cages. The small cell parameters and volume give the shortest ever observed intermolecular C_{60} distances along the 12 first-neighbor fcc directions. These distances are comparable to theoretical ones calculated for C_{60} dimers (*20*) and are characteristic of covalent bonding. The observed ellipse sizes and eccentricities imply a range of different intermolecular distances. For instance, if a diffracting grain has a rhombohedral or a tetragonal cell distortion (Table 1), it will display two different values of intermolecular distance: ~8.80 and ~8.40 Å. Consequently, the 12 observed intermolecular distances are shorter than those measured in 1D and 2D C_{60} polymers and indicate a covalent bonding in all three directions and the formation of 3D polymers. Comparison with the theoretical intermolecular distances calculated for C_{60} dimers (*20*) suggests that the chemical bonds present in these samples may be the result of 2+2 cycloaddition reactions associated with a deformation of the C_{60} cages or of a different cycloaddition reaction (2+4, 6+6, and so forth). The latter results in stronger bonds than the 2+2 cycloaddition and could explain the observed larger compression occurring between polymerized planes and the stabilization of the cell deformation induced by nonhydrostatic compression.

The experimental 2D patterns provide us with so few reflections that it is impossible to solve the structure of our bulk sample. However, model structures can be simulated assuming several structural constraints and starting from basic models such as those for 3D-R, 3D-T, and 3D-C structures. Only face-centered reflections are observed. Thus, all C_{60} molecules are equivalent: they either all have the same orientation, or the structure is partly disoriented and we could not distinguish their relative orientation by diffraction. In the 3D-R and 3D-T models (Fig. 2, A through D), C_{60} molecules are fcc equivalent by translation, allowing their corresponding atomic positions to be used for intensity simulations. They agree with the measured intensity only when we introduce some radial distortion of the molecular cage. We have varied the distance between C atom and cage center, maintaining the relative orientation of C atoms in each molecule with symmetry constraints in such a way that we have only one to six sets of C atom/cage center distances. For all spectra simulated with these atomic positions, the models require a very large atomic thermal Debye-Waller (D-W) factor ($\langle u^2 \rangle \approx 0.5$ Å^2), and consequently, we could also describe molecules as charge surfaces. However, neither a uniform spherical distribution of atoms (*23*) (as for the pristine C_{60} fcc structure) nor a uniform elliptical one can explain the observed intensities of (00l) fcc reflections. It is evident that the 002 reflection is very intense, whereas the 004 reflection practically disappears (Fig. 1). Simulations of the experimental pattern using simple models such as a sum of Bessel functions, corresponding to different shells of charge, or cylindrical Bessel functions, corresponding to a sum of rings of charge, failed. In our 3D-compressed fullerite phases, we must have molecular radial deformations ($\Delta R/R \approx 12$ to 15%) corresponding to a corrugated cage. This last possibility is compatible with several kinds of bonds having different strengths. Similar agreements were obtained for the three models by using only few sets of C atom/cage center radii (in the range of 3.4 to 4.0 Å). The intramolecular C-C bonding was maintained in the range of 1.4 to 1.6 Å and the shortest intermolecular C-C bonding along the <110> directions was in the range of 1.5 to 1.9 Å. Two 3D-R and 3D-T models are represented (Fig. 2, A and B, and C and D) with C_{60} molecule deformations compatible with our x-ray patterns. The 3D-C model (Fig. 2, E and F), which is not fcc, also correctly fits the observed data when we use large D-W thermal factors and deform the molecules with a similar C atom/cage center radius.

We should stress that these structures differ only by slight molecular rotations. The large D-W thermal factors are compatible with a partial molecular disorientation giving rise to intermediate intermolecule bondings, the molecule deformations being related to the directions of the neighboring cages. This means that carbon atoms lie on a distorted closed surface of radius between 3.4 and 4.0 Å, generating large empty holes. Because of the short range order character of this structure and the weakness of most of Bragg reflections, we have only tried some chemically reasonable models. Although it is probable that other models may give similarly good agreement, we stress that the following points are certain:

(i) Our 2D experimental patterns and simulations show that the C_{60} cage structure is conserved with a cell volume close to the O'Keeffe model (*4*). The intermolecular distances have been strongly reduced, in all three dimensions, to a separation compatible with intermolecular chemical bonding, that is, 3D polymerization. (ii) The molecules present a static orientational disorder. (iii) There is a radial cage deformation together with a cell deformation. The structure is likely to be a continuous network of mainly sp^3 carbon atoms with big cages placed periodically, that is, a carbon zeolite. Cell distortions are related to the nonhydrostatic conditions of compression during synthesis and remain in the sample as a result of the formation of covalent intermolecular bonds. Consequently, the continuous evolution of the cell parameters is related to the grain orientation relative to the loading direction during synthesis and gives rise to "Debye-Scherrer ellipses" which remain after the release of pressure.

Table 1. Lattice parameters, C_{60} intermolecular distances along <110>, and C_{60} average cage radii R_{av} of 3D-C_{60} polymers, extracted from measured D-S ellipses and used for intensity simulations. Letters in parentheses [(a) through (e)] correspond to labeled structures in Fig. 2G.

	3D-R	3D-T	3D-C	Pristine C_{60}	C_{60} dimers (*20*)
Unit cell	a = 12.072 Å α = 93.445°	a = 12.430 Å c = 11.324 Å	a = 12.050 Å	a = 14.158 Å	
C_{60} cage radius	R_{av} = 3.60 Å	R_{av} = 3.63 Å	R_{av} = 3.58 Å	R = 3.548 Å	
C_{60}–C_{60} distance	(a) 8.79 Å (b) 8.28 Å	(c) 8.79 Å (d) 8.41 Å	(e) 8.52 Å	10.01 Å	(2+2) 9.2 Å (2+4) 8.7 Å (6+6) 8.38 Å

References

1. See for example, M. Nicol and G. Z. Yin, *J. Phys. (Paris)* **45-C8**, 163 (1984).
2. M. Núñez-Regueiro, L. Marques, J.-L. Hodeau, O. Béthoux, M. Perroux, *Phys. Rev. Lett.* **74**, 278 (1995).
3. Y. Iwasa *et al.*, *Science* **264**, 1570 (1994).
4. M. O'Keeffe, *Nature* **352**, 674 (1991).
5. M. Núñez-Regueiro, L. Marques, J.-L. Hodeau, C.-H. Xu, G. Scuseria, *Fullerene Polymers and Fullerene-Polymer Composites*, A. Rao and P. C. Eklund, Eds. (Springer-Verlag, Berlin), chapter 7, in press.
6. L. Marques, J.-L. Hodeau, M. Núñez-Regueiro, M. Perroux, *Phys. Rev. B* **54**, R12663 (1996); V. Agofonov *et al.*, *Chem. Phys. Lett.* **267**, 193 (1997); R. Moret, P. Launois, P. A. Persson, B. Sundqvist, *Europhys. Lett.* **40**, 55 (1997).
7. C. S. Yoo and W. J. Nellis, *Science* **254**, 1489 (1991).
8. M. Núñez-Regueiro, P. Monceau, J.-L. Hodeau, *Nature* **355**, 237 (1992).
9. H. Hirai, K. Kondo, T. Ohwada, *Carbon* **31**, 1095 (1993).
10. J.-L. Hodeau *et al.*, *Phys. Rev. B* **50**, 10311 (1994).
11. H. Hirai, Y. Tabira, K. Y. Kondo, T. Oikawa, N. Yoshizawa, *ibid.* **55**, 15555 (1995).
12. V. D. Blank *et al.*, *Phys. Lett. A* **205**, 208 (1995); V. D. Blank *et al.*, *ibid.* **220**, 149 (1996).
13. V. D. Blank, B. A. Kulnitskiy, Ye V. Tatyanin, O. M. Zhigalina, *EMAG'97 Proceedings*, in *Inst. Phys. Conf. Ser.* **153**, 593 (1997).
14. D. Häusermann *et al.*, *ESRF Newsletters* **30**, 25 (1998).
15. M. Thoms *et al.*, *Nucl. Instrum. Methods Phys. Res. A* **413**, 175 (1998).
16. A. Hammersley, O. Svensson, M. Hanfland, A. Fitch, D. Häusermann, *High Pressure Res.* **14**, 235 (1996).
17. G. Kinsland and W. Bassett, *Rev. Sci. Instrum.* **47**, 130 (1976).
18. N. Funamori, T. Yagi, T. Uchida, *J. Appl. Phys.* **75**, 4327 (1994).
19. A. Singh, *ibid.* **73**, 4278 (1993).
20. D. Strout *et al.*, *Chem. Phys. Lett.* **214**, 576 (1993); C. H. Xu and G. E. Scuseria, personal communication.
21. W. I. F. David, R. M. Ibberson, T. J. Dennis, J. P. Hare, K. Prassides, *Europhys. Lett.* **18**, 219 (1992); *ibid.*, p. 735.
22. W. I. F. David and R. M. Ibberson, *J. Phys. Condens. Matter* **5**, 7923 (1993); B. Sundqvist, O. Andersson, A. Lundin, A. Soldatov, *Solid State Commun.* **93**, 109 (1995); J. A. Wolk, P. J. Horoyski, M. L. W. Thewalt, *Phys. Rev. Lett.* **74**, 3483 (1995).
23. J. Fischer *et al.*, *Science* **252**, 1288 (1991).

9 September 1998; accepted 3 February 1999